Supplementary Methods

Dual-mode detection for the total antioxidant capability of skincare products based on porous CuS@CdS@Au nanoshells

Weimin Yang, Qi Ding, Xinhe Xing, Fang Wang, Hengwei Lin, Si Li*

EXPERIMENTAL SECTION

Chemicals and Materials

Copper chloride ($CuCl_2 \cdot 2H_2O$), polyvinylpyrrolidone (PVP-K30), sodium hydroxide (NaOH), hydrazine hydrous solution ($N_2H_4 \cdot H_2O$), sodium sulfide ($Na_2S \cdot 9H_2O$), cadmium perchlorate hexahydrate ($Cd(ClO_4)_2 \cdot 6H_2O$), thioacetamide (TAA), hydrogen tetrachloroaurate (III) ($HAuCl_4 \cdot 3H_2O$), Sodium borohydride ($NaBH_4$), 3,3',5,5'- tetramethylbenzidine dihydrochloride hydrate (TMB), ascorbic acid (AA), glutathione (GSH), ferulic acid (FA), hydrogen peroxide (H_2O_2, 30%), acetic acid (CH_3COOH), sodium acetate trihydrate (CH_3COONa), zinc chloride, cobalt chloride, magnesium sulfate, potassium chloride, sodium chloride, nickel chloride, chromic nitrate, serine, tartaric acid, proline, lysine, cysteine, and histidine were purchased from Aladdin chemical reagent (Shanghai, China). All reagents were analytical grade and without further purification. Ultrapure water with a resistivity of 18.2 MΩ·cm was used throughout the experiments.

Instrumentation

TEM images were performed with a Talos F200X G2 scanning transmission electron microscope (Thermo Fisher Scientific, USA) at an acceleration voltage of 200 kV. Powder XRD patterns were collected with a Bruker D8 diffractometer equipped with a Cu Kα radiation source (40 kV, 40 mA) at a rate of 5°/min. XPS was obtained from Axis Supra (Kratos, UK). Inductively coupled plasma-mass spectrometry (ICP-MS) was taken on an ICAP TQ (Thermo Fisher Scientific, USA). Size distributions were obtained with a Zetasizer (Malvern Instruments Ltd., Malvern, UK). All UV-

visible absorption spectra were determined with a Shimadzu UV-vis 3101 spectroscope. The catalytic activities were determined using SpectraMax M2 Microplate Readers (Molecular Devices, USA). Electronic spin resonance (ESR) was obtained using EMXplus-10/12 from Bruker Technology GmbH (Karlsruhe, Germany). The laser source for the 808 nm photoexcitation was FC-808/980-10W (CNI, China).

Synthesis of porous CuS nanoshells

Porous CuS nanoshells (NSs) were synthesized using the previously reported method with minor modifications.[1] Briefly, 16 μL $CuCl_2$ solution (0.5 M) was added to 10 mL deionized water containing 48 mg PVP-K30 under magnetic stirring at room temperature. Then, 50 μL 1 mM NaOH solution was injected into the pre-prepared solution, followed by adding 30 μL $N_2H_4 \cdot H_2O$ (8.5%) to form a bright-yellow suspension of Cu_2O spheres. After reacting for 10 min, 36 μL Na_2S aqueous solution (320 mg mL^{-1}) was added and heated for 2 h at 60 °C. Finally, CuS nanoshells were centrifuged at 9000 rpm for 10 min and washed three times using deionized water. Then, the supernatant was removed, and the CuS precipitation was dispersed in 5 mL of deionized water.

Synthesis of CuS@CdS nanoshells

250 μL of 1 mM $Cd(ClO_4)_2 \cdot 6H_2O$ was added to 5 mL of CuS solution and stirred for 10 min. Then, 225 μL of 10 mM TAA was added to the above solution under stirring. After 10 min, 250 μL of 0.85% $N_2H_4 \cdot H_2O$ was added to the suspension under stirring for 10 min. Finally, CuS@CdS were centrifuged at 5000 rpm for 10 min and washed three times with deionized water. Then, the supernatant was removed, and the CuS@CdS nanoshells were dispersed in 5 mL of deionized water.

Synthesis of CuS@CdS@Au nanoshells

12 mg PVP-K30 was added to 1 mL of CuS@CdS solution and stirred for 30 min. After that, 4 mL $HAuCl_4 \cdot 3H_2O$ aqueous solution (0.3 mM) was added and stirred for 10 min. In the following, 0.5 mL $NaBH_4$ (3 mM) was added and stirred for another 30 min. The products were collected by centrifugation at 5000 rpm for 10 min and washed

three times with deionized water. Then, the supernatant was removed, and the CuS@CdS@Au nanoshells were dispersed in 1 mL of deionized water.

Enzyme-like activity of CuS@CdS@Au nanoshells

Typically, 20 μL CuS@CdS@Au (the concentration of Cu elements used for the catalysis evaluation was 60 ppm (**Table S1**)) was added to a mixture containing 40 μL of acetate buffer (pH 4.0), 20 μL of H_2O_2 (10 mM), 20 μL of TMB (5 mM). After irradiation for 5 min using 808 nm laser, the absorption spectra of the above mixture were measured by a UV−Vis spectrophotometer. Meanwhile, the solutions were photographed by a smartphone, and the temperature of the solutions was recorded by a thermal imager.

Colorimetric and temperature detection of TAC by CuS@CdS@Au

Typically, 20 μL of AA/GSH/FA standard solution with different concentrations was added to a mixture containing 20 μL of acetate buffer (pH 4.0), 20 μL of H_2O_2 (10 mM, 20 μL of TMB (5 mM), 20 μL of CuS@CdS@Au (the concentration of Cu was 60 ppm). After irradiation for 5 min using 808 nm laser, the absorption spectra of the above mixture were measured by a UV−Vis spectrophotometer. Meanwhile, the solutions were photographed by a smartphone, and the temperature of the solutions was recorded by a thermal imager. Quantitative detection of AA/GSH/FA was achieved by establishing a linear relationship between the absorbance intensity at 652/450 nm or the temperature and the concentrations of TAC.

Evaluation of the catalytic ability of CuS, CuS@CdS and CuS@CdS@Au nanoshells

The catalytic activity of CuS, CuS@CdS, and CuS@CdS@Au was evaluated based on the oxidation of TMB in the presence of H_2O_2. First, H_2O_2 and TMB solutions were mixed with the acetate buffer (pH 4.0). Next, CuS, CuS@CdS, and CuS@CdS@Au solutions were added to the above solution. The final concentration of H_2O_2 was 2 mM; the final concentrations of TMB were 0.5, 1, 1.25, 2.5, 5, and 10 mM. After irradiation for 5 min using an 808 nm laser, the absorption spectra of the above-mixed detection samples were measured by a UV−Vis spectrophotometer.

The initial reaction rates (V) were measured first by the time-dependent absorbance changes (652nm) ($\varepsilon_{652\ nm}$=39,000 M^{-1} cm^{-1}) of TMB (0.5, 1, 1.25, 2.5, 5, 10 mM). The Michaelis-Menten kinetics curves of CuS, CuS@CdS, and CuS@CdS@Au were plotted according to the average values of V versus the concentrations of TMB. The Lineweaver-Burk plots of CuS, CuS@CdS, and CuS@CdS@Au were plotted according to the values 1/V versus the concentrations of TMB. The kinetic parameters of V_{max} and K_m were calculated based on the Michaelis-Menten equation ($V = (V_{max} \times [S]) / (K_m + [S])$). All measurements were repeated at least three times for accuracy.[2, 3]

The catalytic activity of CuS, CuS@CdS, and CuS@CdS@Au was evaluated by catalyzing the oxidation of TMB in the presence of H_2O_2. First, H_2O_2 and TMB solutions were mixed with acetate buffer (pH 4.0). Next, CuS, CuS@CdS, and CuS@CdS@Au solution was added to the above solution. The final concentration of TMB was 1 mM; the final concentrations of H_2O_2 were 1.25, 2.5, 5, 10, 20, and 30 mM. After irradiation for 5 min using an 808 nm laser, the absorption spectra of the above-prepared samples were measured by the UV−vis spectrophotometer.

Calculation and Analysis of LOD

The LOD was calculated via sensitivity analysis. The calibration curve was resented as:

$$Y = a + bX$$

where a and b are variables obtained through least-squares linear regression of the signal–concentration curve and variable Y represents the absorbance/temperature intensity of CuS@CdS@Au at an AA/GSH/FA concentration of X (μM), and X is equal to log C.

The LOD was calculated as follows:

When b > 0,

$$Y = C_{blank} + 3\times SD$$

$$LOD=10\times \frac{\left(C_{blank} + 3 \times SD\right) - a}{b}$$

where SD is the standard deviation and C_{blank} is the absorbance/temperature intensity of the blank sample (without AA/GSH/FA) and SD is the standard deviation.

When b < 0

$$Y = C_{blank} - 3 \times SD$$

$$LOD = 10 \times \frac{(C_{blank} - 3 \times SD) - a}{b}$$

SD was calculated based on the formula:

$$SD = \sqrt{\frac{1}{N_r - 1} \times \sum_{i=1}^{N_r} (X_i - X_{avg})^2}$$

N_r: total number of samples;

X_i: the absorbance intensity of each sample;

X_{avg}: average value for the absorbance/temperature intensity obtained for a specific series of identical samples repeated N_r times.

Analysis for Real Samples

Recovery experiments were performed to assess the accuracy of the method. A 9mL blank skincare sample without antioxidants was mixed with 1mL 1 mM FA standard solution (final concentration of FA was 100 μM). The resulting solution was vortexed and then analyzed using the Dual-mode detection of TAC.

$$\text{Recovery (\%)} = \frac{amount\ in\ spike\ sample\ -\ amount\ in\ sample}{amount\ in\ spike} \times 100$$

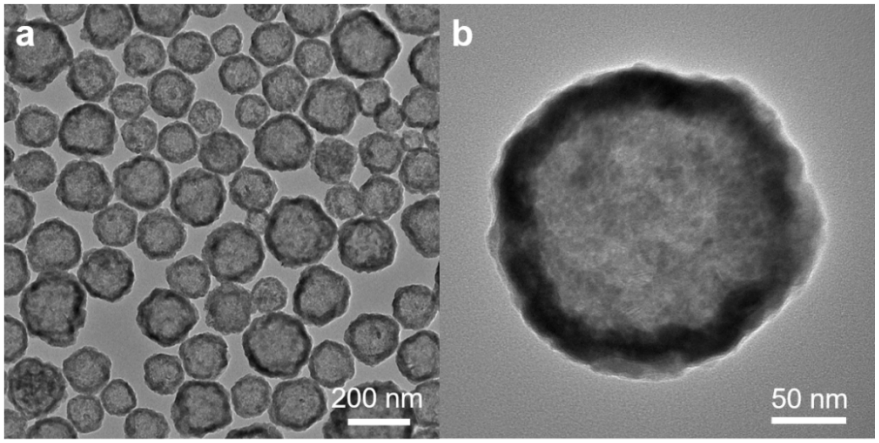

Fig. S1. (**a-b**) Transmission electron microscope (TEM) images of CuS nanoshells.

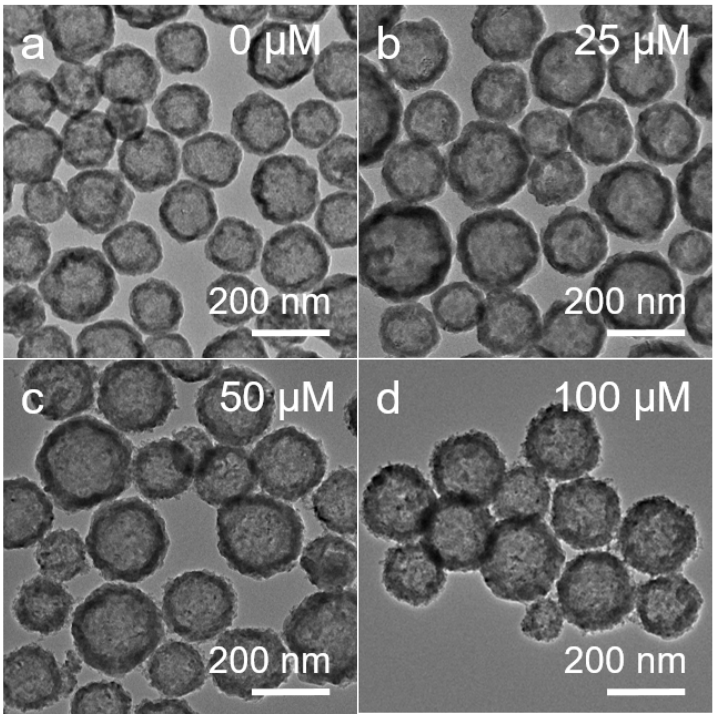

Fig. S2. Transmission electron microscope (TEM) images of CuS@CdS constructing with (**a**) 0 μM Cd^{2+}, (**b**) 25 μM Cd^{2+}, (**c**) 50 μM Cd^{2+}, (**d**) 100 μM Cd^{2+}.

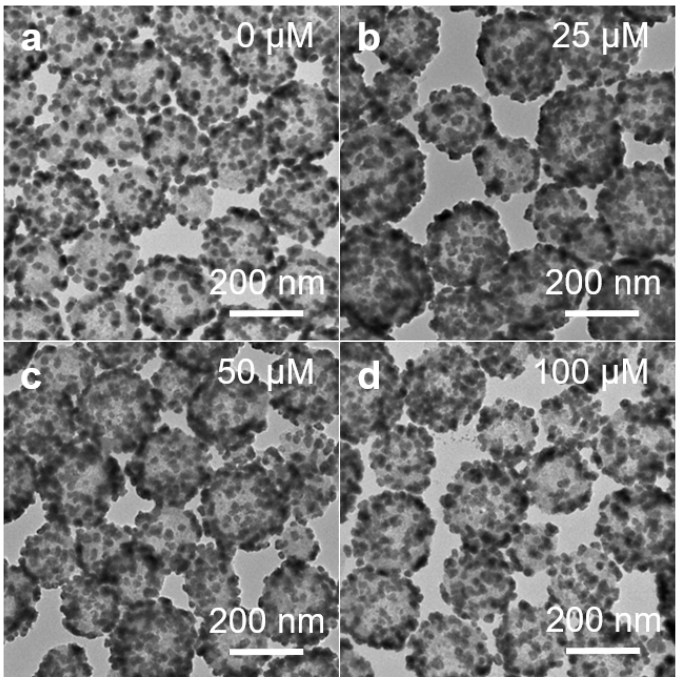

Fig. S3. Transmission electron microscope (TEM) images of CuS@CdS@Au constructing with (**a**) 0 μM Cd^{2+}, (**b**) 25 μM Cd^{2+}, (**c**) 50 μM Cd^{2+}, (**d**) 100 μM Cd^{2+}.

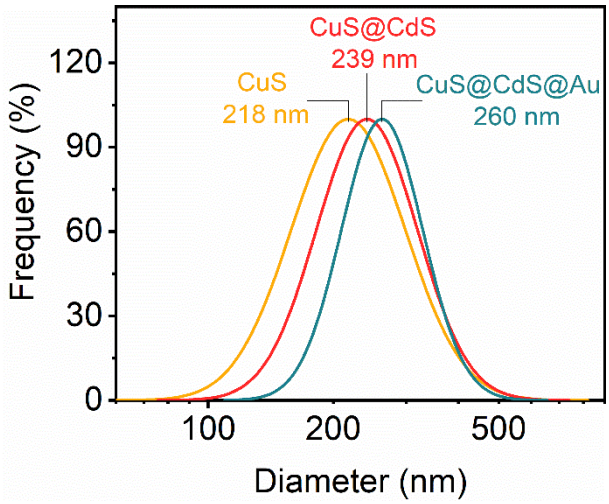

Fig. S4. Size distribution of CuS, CuS@CdS, and CuS@CdS@Au.

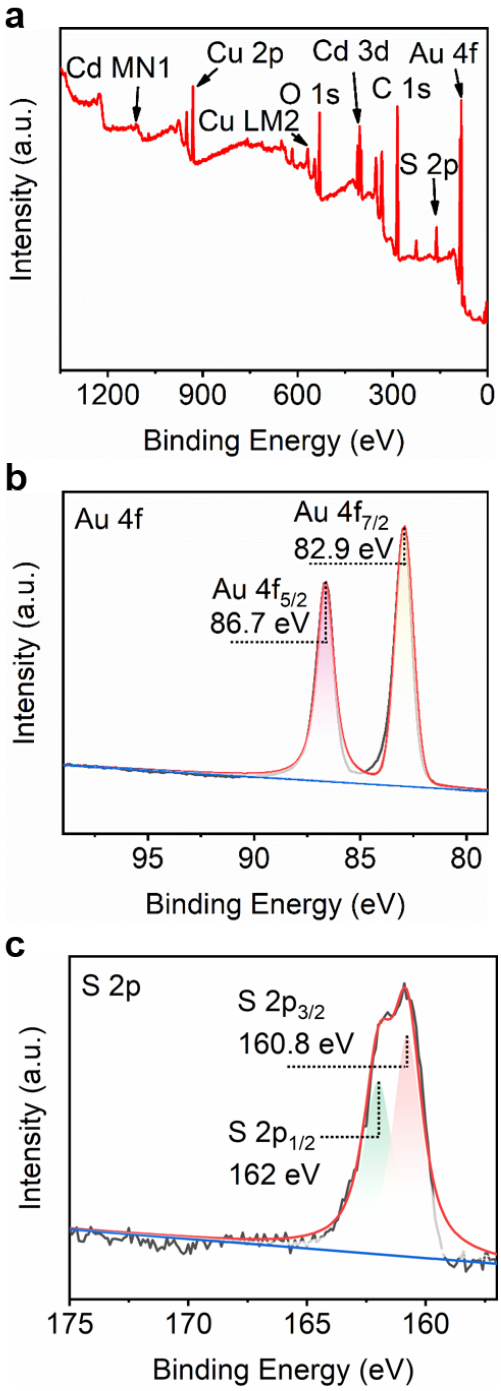

Fig. S5. (**a**) XPS survey spectrum of CuS@CdS@Au nanoshells. (**b**) High-resolution XPS spectrum of Au in CuS@CdS@Au nanoshells. (**c**) High-resolution XPS spectrum of S in CuS@CdS@Au nanoshells.

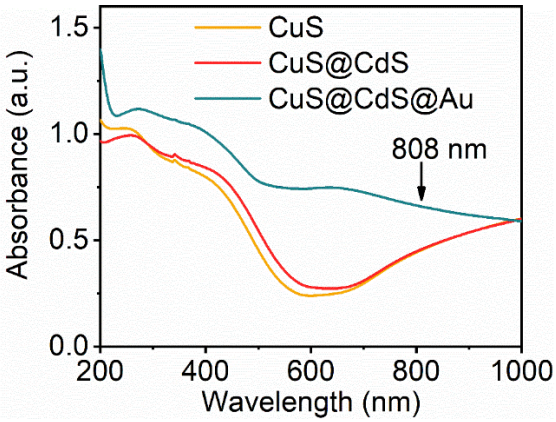

Fig. S6. UV-visible absorption spectra of CuS, CuS@CdS, and CuS@CdS@Au nanoshells.

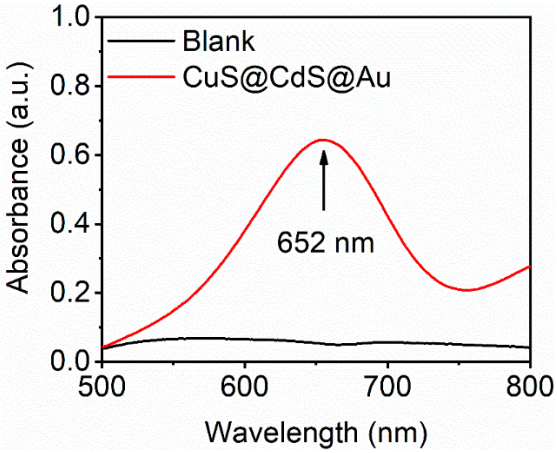

Fig. S7. UV-visible absorption spectra of TMB after being photocatalyzed with or without CuS@CdS@Au (blank) in the presence of H_2O_2.

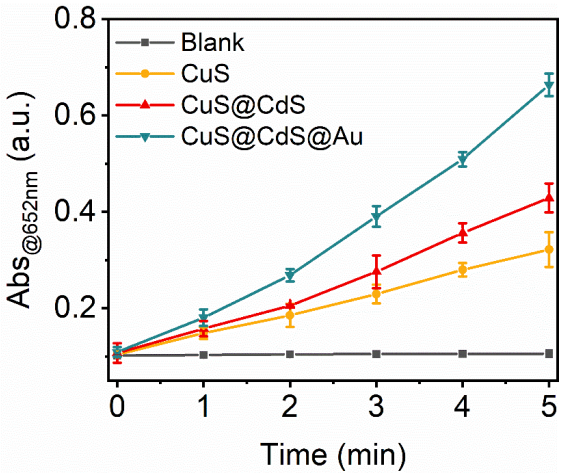

Fig. S8. Absorption intensities (652 nm) of TMB were obtained after being photoirridated with or without CuS, CuS@CdS, and CuS@CdS@Au at different times in the presence of H_2O_2.

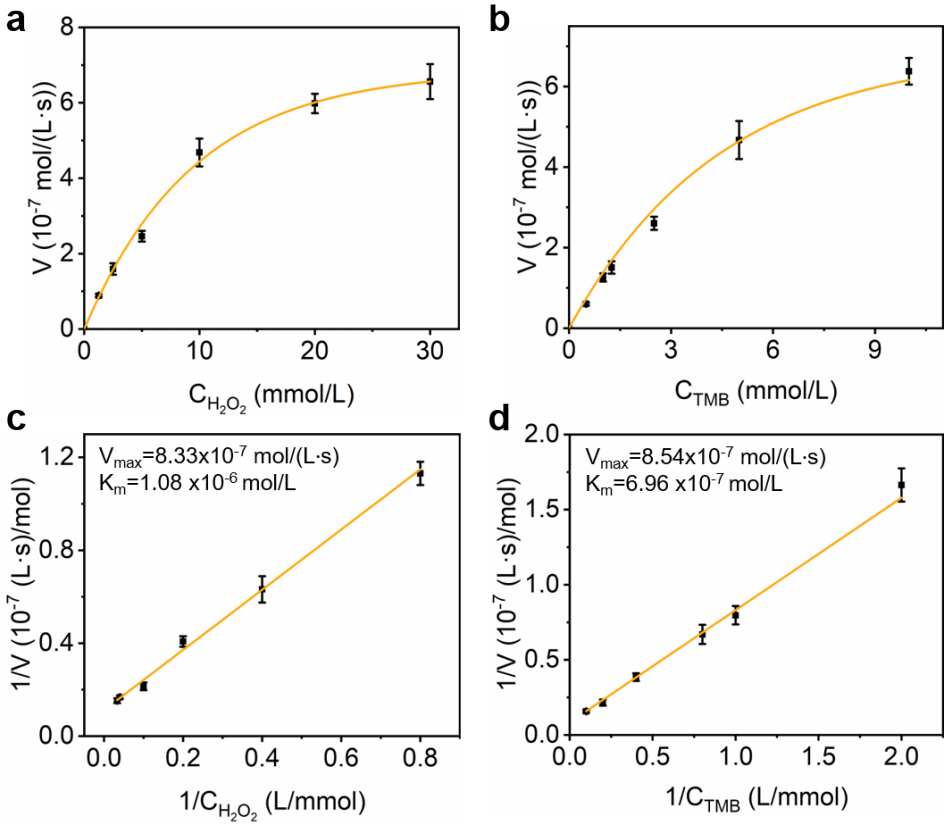

Fig. S9. (**a, b**) Kinetic studies on the catalytic oxidation of TMB in the presence of H_2O_2 and CuS under NIR light irradiation. (**c, d**) The plots of the corresponding double reciprocal of the Michaelis-Menten equations.

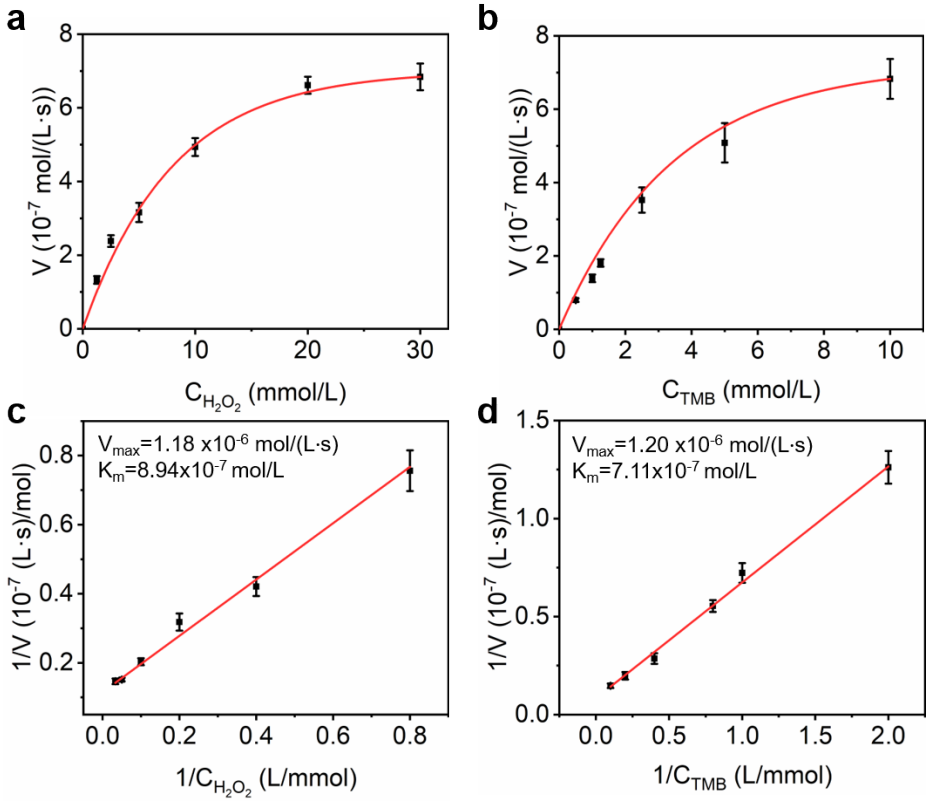

Fig. S10. (**a, b**) Kinetic studies on the catalytic oxidation of TMB in the presence of H_2O_2 and CuS@CdS under NIR light irradiation. (**c,d**) The plots of the corresponding double reciprocal of the Michaelis-Menten equations.

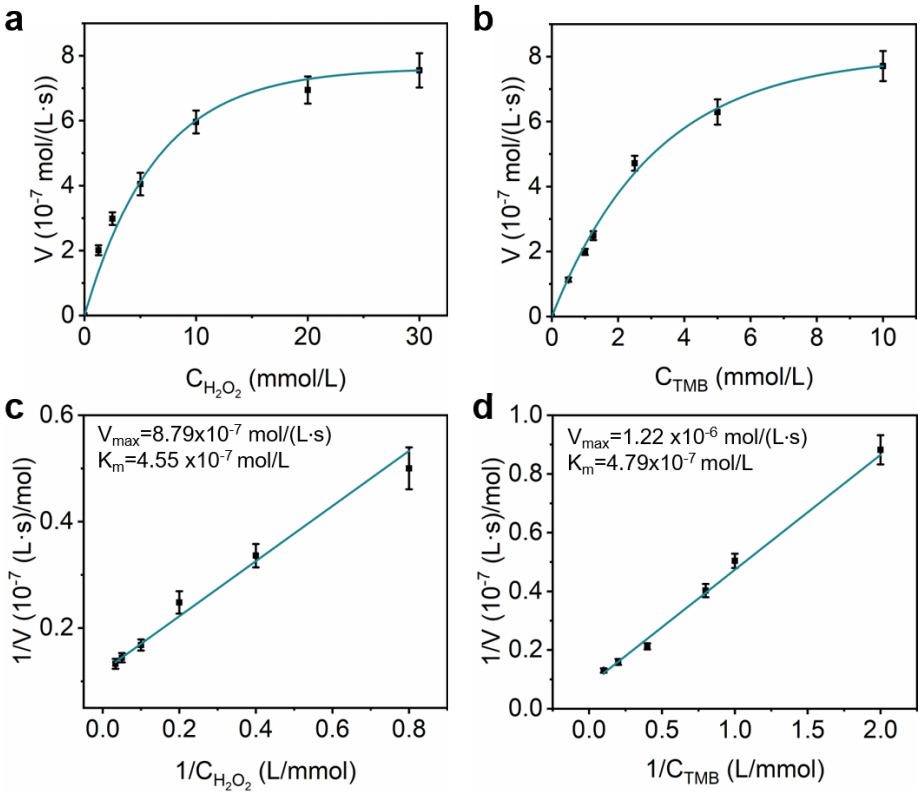

Fig. S11. (**a**, **b**) Kinetic studies on the catalytic oxidation of TMB in the presence of H_2O_2 and CuS@CdS@Au under NIR light irradiation. (**c**, **d**) The plots of the corresponding double reciprocal of the Michaelis-Menten equations.

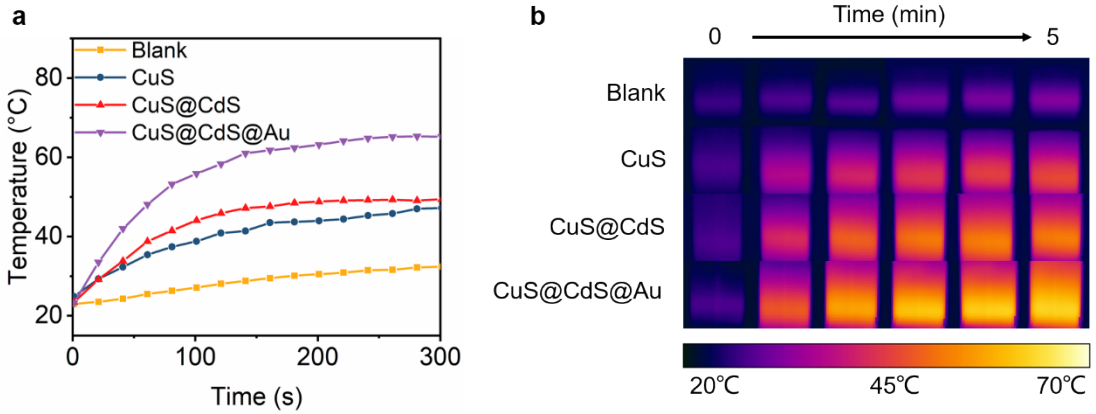

Fig. S12. (**a**) Temperature curve of Blank, CuS, CuS@CdS, and CuS@CdS@Au (the concentration of Cu is 60 ppm) after being irradiated by 808 nm laser for 5 min (0.5 W/cm^2). (**b**) Photothermal images obtained during photoirradiation.

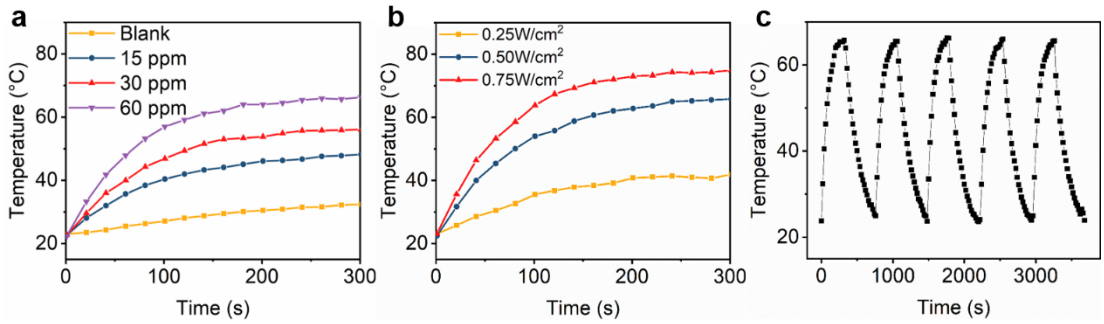

Fig. S13. (**a**) Temperature curve of CuS@CdS@Au with different concentrations. (**b**) Temperature curve of CuS@CdS@Au with different power densities. (**c**) Photothermal stability of CuS@CdS@Au upon five cycles of the on/off NIR laser.

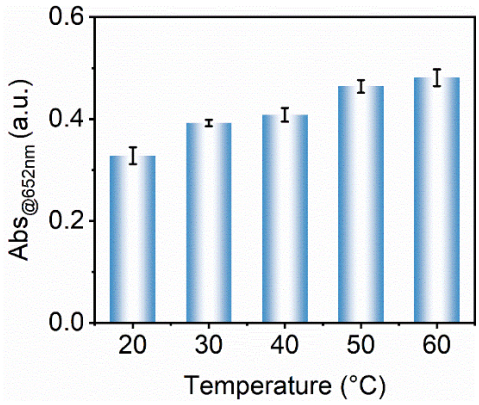

Fig. S14. Temperature effect on the peroxidase-like activity of CuS@CdS@Au.

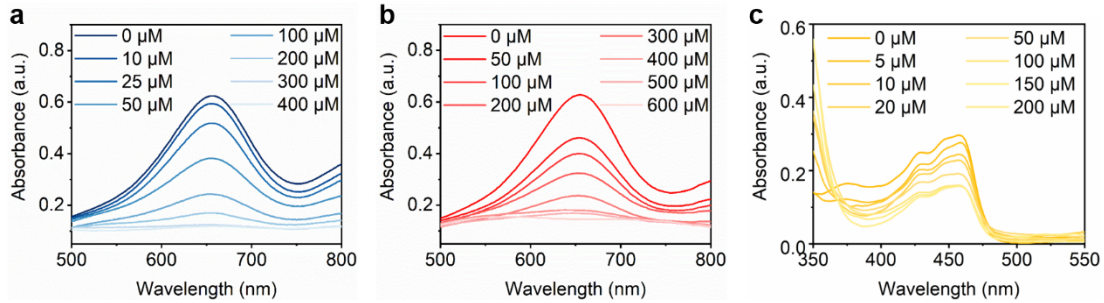

Fig. S15. Absorbance responses of CuS@CdS@Au toward different concentrations of (**a**) AA, (**b**) GSH, and (**c**) FA, respectively.

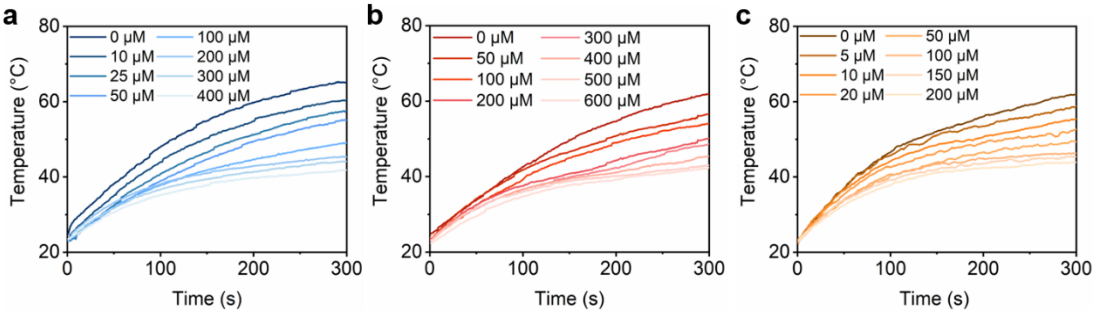

Fig. S16. Temperature responses of CuS@CdS@Au toward different concentrations of (**a**) AA, (**b**) GSH, and (**c**) FA, respectively.

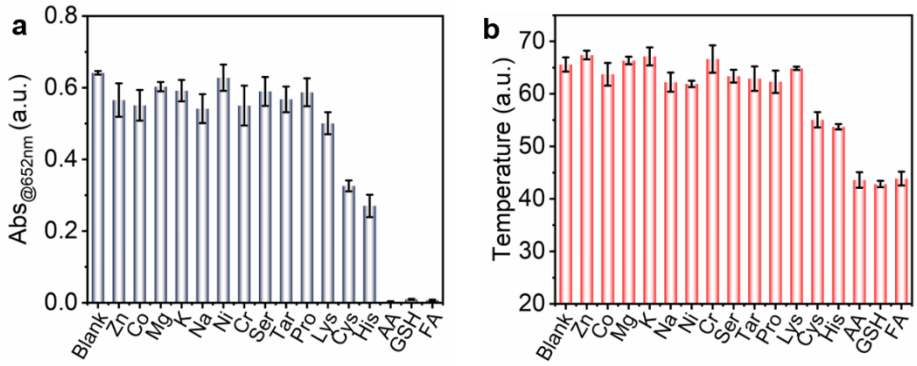

Fig. S17. Anti-interference tests for antioxidant detection.

Table S1. The molar ratio of Cu, Cd, and Au was measured by ICP-MS.

Sample	Cu (ppm)	Cd (ppm)	Au (ppm)
CuS	64.29	/	/
CuS@CdS	62.83	8.03	/
CuS@CdS@Au	60.08	7.89	67.37

Table S2. Comparison of steady-state kinetic data for catalytic oxidation of TMB in the presence of H_2O_2 with NIR irradiation (808 nm laser).

	Substrate	CuS	CuS@CdS	CuS@CdS@Au
Km	TMB	8.94×10^{-7}	7.11×10^{-7}	4.79×10^{-7}
(mol/L)	H_2O_2	1.08×10^{-6}	6.96×10^{-7}	4.55×10^{-7}
V_{max}	TMB	1.18×10^{-6}	1.20×10^{-6}	1.22×10^{-6}
(mol/(L·s))	H_2O_2	8.33×10^{-7}	8.54×10^{-7}	8.79×10^{-7}

References

1. X. Deng, K. Li, X. Cai, B. Liu, Y. Wei, K. Deng, Z. Xie, Z. Wu, P. Ma, Z. Hou, Z. Cheng and J. Lin, *Adv. Mater.*, 2017, **29**, 1701266.
2. S. Li, F. Wang, X. Xing, X. Yue, S. Sun, H. Lin and C. Xu, *Adv. Healthc. Mater.*, 2024, **13**, e2303476.
3. B. Jiang, D. Duan, L. Gao, M. Zhou, K. Fan, Y. Tang, J. Xi, Y. Bi, Z. Tong, G. F. Gao, N. Xie, A. Tang, G. Nie, M. Liang and X. Yan, *Nat. Protoc.*, 2018, **13**, 1506-1520.